

10-MW-level peak power Mamyshev oscillator enabled by anti-resonant hollow-core fiber

Shan Wang^{1,2,3}, Di Lin^{1,2,3}, Xin Zhang⁴, Ziheng Zhuang^{1,2,3}, Weijia Luo^{1,2,3}, Cong Zhang^{1,2,3},
Meng Xiang^{1,2,3}, Jianping Li^{1,2,3}, Songnian Fu^{1,2,3}, Pu Wang⁴ and Yuwen Qin^{1,2,3}

¹*Institute of Advanced Photonics Technology, School of Information Engineering, Guangdong University of Technology, Guangzhou, 510006, China*

²*Key Laboratory of Photonic Technology for Integrated Sensing and Communication, Ministry of Education of China, Guangdong University of Technology, Guangzhou, 510006, China*

³*Guangdong Provincial Key Laboratory of Information Photonics Technology, Guangdong University of Technology, Guangzhou, 510006, China*

⁴*Institute of Laser Engineering, Beijing Engineering Research Center of Laser Applied Technology, Beijing University of Technology, Beijing, 100124, China*

Correspondence to: D. Lin and Y. Qin, School of Information Engineering, Guangdong University of Technology, Guangzhou, 510006, China. Emails: dilin@gdut.edu.cn; qinyw@gdut.edu.cn

Abstract Mamyshev oscillators (MOs) demonstrate extraordinarily superior performance compared with fiber laser counterparts. However, the realization of a fully fiberized, monolithic laser system without pulse degradation remains a key challenge. Here we present a high-energy MO using large mode area Yb-doped fiber and fiber-integrable interferometric super-Gaussian spectral filters, that directly generates a nearly diffraction-limited beam with ~9.84 W average power and ~533 nJ pulse energy. By implementing pre-chirp management

This peer-reviewed article has been accepted for publication but not yet copyedited or typeset, and so may be subject to change during the production process. The article is considered published and may be cited using its DOI.

This is an Open Access article, distributed under the terms of the Creative Commons Attribution licence (<https://creativecommons.org/licenses/by/4.0/>), which permits unrestricted re-use, distribution, and reproduction in any medium, provided the original work is properly cited.

10.1017/hpl.2025.31

with anti-resonant hollow-core fiber (AR-HCF), the adverse effects of super-Gaussian filtering on pulse quality are effectively mitigated, enabling pulse compression to 1.23 times the transform limit. Furthermore, AR-HCF is employed to provide negative dispersion to compensate for the positive chirp of output pulses, resulting in ~ 37 fs de-chirped pulses with ~ 10 MW peak power. This approach represents a significant step toward the development of monolithic fiber lasers capable of generating and flexible delivery of sub-50-fs pulses with tens of megawatts peak power.

Key words: Mamyshev oscillator, anti-resonant hollow-core fiber, pre-chirp management, fiber pulse compression

I. INTRODUCTION

Mode-locked fiber lasers have been attracting considerable interest in various industrial and scientific fields due to their robust operation, compact size, high optical efficiency and cost effective [1]. A critical challenge encountered by these systems is the enhancement of peak power, necessitating the achievement of higher pulse energies and shorter pulse durations. However, the intrinsic properties of fiber lasers, particularly their tight mode confinement and extended propagation length, lead to significantly nonlinear effects that ultimately destabilize pulse evolution, thereby restricting the achievable peak power to levels considerably lower than those attainable with bulk solid-state lasers. Over the past few decades, researchers have developed several advanced techniques to effectively manage these nonlinearities, including dispersion-managed fiber lasers [2], self-similar fiber lasers [3], and all-normal dispersion fiber lasers [4]. These strategies typically yield maximum pulse energies of approximately 20 nJ with sub-100-fs pulse durations in single-mode fibers (SMFs) [4]. Recent advancements in fiber-based Mamyshev

oscillators (MOs) have exhibited markedly superior performance compared to other fiber-based systems, especially in their capability to directly generate megawatt-level peak power pulses from SMF oscillators [5]. Moreover, the incorporation of specially designed ultra-low numerical aperture (NA) large mode area Yb-doped fiber (LMA-YDF) and Yb-doped photonic crystal fiber (YD-PCF) has facilitated the achievement of pulse energies exceeding 1 μJ , with externally compressed pulse durations of approximately 50 fs and peak powers surpassing 10 MW. This advancement represents an order of magnitude improvement over traditional mode-locked fiber lasers [6,7].

The exceptional performance of MOs can be primarily attributed to the parabolic pulse evolution, in conjunction with the step-like effective saturable absorber created by the integration of two central-wavelength-offset bandpass filters. This configuration facilitates the generation of stable mode-locked pulses even under the condition of an accumulated nonlinear phase shift of $\sim 60\pi$ [5]. The Gaussian-shaped transmission profile of the spectral filters plays a pivotal role in scaling pulse energies and achieving high-quality pulse compression, generally resulting in compressed pulse durations around 1.6 times the transform-limited (TL) duration at microjoule-scale pulse energies [6,7]. However, the implementation of Gaussian-shaped filters typically necessitates the incorporation of a diffraction grating, along with a collimator and a section of SMF, resulting in a cumbersome configuration that is impractical for fiber integration. Consequently, compactly fiber-integrated interferometric spectral filters featuring a near super-Gaussian transmission profile have become a common choice in fully fiberized MOs. Nevertheless, these MOs generally exhibit inferior performance compared to those employing Gaussian-shaped spectral filters. For instance, a MO utilizing a 10 μm core diameter polarization maintaining (PM) YDF in conjunction with Gaussian-shaped spectral filters is capable of

generating stable pulses with energies of 190 nJ, further compressed to 35 fs (~ 1.25 times the TL duration), achieving a peak power of 3 MW [8]. In contrast, a MO employing super-Gaussian filters with an equivalent core diameter of PM-YDF produces pulses of only ~ 83 nJ, compressed to 56 fs (~ 2.8 times the TL duration) with a peak power of 1.15 MW [9]. This performance penalty indicates the incomplete parabolic pulse evolution associated with the latter configuration. The superior performance of Gaussian-shaped filters can be attributed to their smoother spectral transmission profile, which facilitates parabolic pulse evolution more effectively. It is well established that optimizing pre-chirp is essential for accelerating pulse evolution toward an asymptotic parabolic regime within self-similar fiber amplifiers, allowing for high-quality pulse compression [10-12]. Given that pulse evolution is inherently dependent on the amplifier gain parameters, the optimal pre-chirp is contingent upon pulse energies. For example, a nearly TL 38-fs pulse with minimal pedestal at a pulse energy of 1.2 μJ has been achieved from a negatively pre-chirped self-similar YDF amplifier [13]. In conventional MOs which comprise two cascaded YDF amplifiers, it is essential that the pulses within each amplifier evolve toward a parabolic shape. Therefore, it is anticipated that the implementation of pre-chirp management within MOs could potentially benefit the evolution of pulses into a parabolic shape with a linear chirp even when employing super-Gaussian filters. In addition, a recent study shows that effective intracavity pre-chirp management can improve the achievable pulse energy in the MO [14].

The output pulses from MOs typically exhibit a slight positive linear chirp over their broadband spectrum, which is commonly compensated for through the utilization of a bulky grating-based compressor to achieve sub-50-fs pulses with megawatt-level peak powers. However, numerous applications, such as micro-machining [15], in vivo and in situ nonlinear imaging [16-18], and microsurgery [19,20] demand the flexible delivery of high-peak-power femtosecond

pulses over several meters of optical fiber with minimal attenuation and distortion at the target. This capability is especially critical in contexts like laser surgery, where the laser source may need to be positioned at a considerable distance from the operational site to provide a more organized and efficient working environment for surgeons. Therefore, the development of a fiber-based compressor capable of effectively delivering microjoule-scale pulse energies over several meters, while maintaining sub-50 fs pulse durations at the fiber output is highly desirable for advancing monolithic MOs.

Conventional solid-core fibers, including LMA fibers and solid core PCFs, have been utilized for pulse compression; however, their applicability is fundamentally constrained to pulse energies of only a few nanojoules due to strong nonlinear effects and low material damage thresholds [21,22]. In contrast, the advanced microstructured hollow-core fibers (HCFs) offer a highly promising alternative. The ambient air-filled cores of HCFs exhibit nonlinearities approximately two orders of magnitude lower than those of silica glass. Additionally, HCFs support fundamental mode operation with a larger effective mode area and possess a significantly higher damage threshold due to their extremely low mode overlap with surrounding silica structures. These properties make HCFs particularly well-suited for both pulse compression and the flexible transmission of high-peak-power femtosecond pulses. Notably, recent investigations into photonic-bandgap HCFs and Kagome-style HCFs have demonstrated remarkable results in the realm of self-compression, achieving few-cycle pulses with energy levels reaching hundreds of microjoules, across wavelengths from ultraviolet to mid-infrared [23-25]. However, the necessity for bulky gas chambers remains a major limitation, significantly undermining the operational flexibility of these systems.

For ultrafast pulses with relatively low pulse energies, the implementation of negative dispersion in air-filled HCFs to directly compensate for the intrinsic positive chirp of laser pulses offers a more straightforward and efficient strategy for pulse compression, all while minimizing nonlinear effects. This approach not only simplifies pulse compression but also enables the flexible transmission of high peak-power femtosecond pulses. Significant efforts have been dedicated to developing monolithic ultrafast laser systems that incorporate air-filled HCF pulse compressors, allowing for the direct generation of femtosecond pulses with durations of hundreds of femtoseconds and peak powers of sub-megawatt [18,26,27]. Recent advancements in anti-resonant HCFs (AR-HCFs) have demonstrated both a reduction in mode overlap with the surrounding glass structures to approximately 10^{-4} to 10^{-5} and a flattening of the anomalous dispersion profile around $1\ \mu\text{m}$. Additionally, these fibers exhibit remarkably low transmission losses, typically below $1\ \text{dB/km}$ around $1\ \mu\text{m}$ [28-30]. These characteristics make AR-HCFs highly promising candidates for such applications.

In this paper, we present a high-energy MO based on commercially available PM LMA-YDF, incorporating several unique design elements that yield exceptional pulse performance. Instead of using conventional bulky grating-based Gaussian-shaped spectral filters typically employed to form the effective saturable absorber, we incorporate more compact, fiber-integrable interferometric spectral filters. To address the challenges associated with the super-Gaussian transmission profile in parabolic pulse evolution, pre-chirp management with optimized group delay dispersion (GDD) is implemented with the assistance of a precisely chosen length of AR-HCF. This configuration facilitates the generation of linearly chirped pulses with high pulse energy. The MO can reach an average output power of $9.84\ \text{W}$ at a repetition rate of $18.46\ \text{MHz}$, corresponding to pulse energies of $533\ \text{nJ}$. Pulse compression is realized by transmitting the pulses

through an optimized length of air-filled AR-HCF, where the positive chirp of the input pulse is effectively compensated by the matched anomalous dispersion provided by the HCF, resulting in a compressed pulse duration of approximately 37 fs and a peak power of 10 MW level.

II. EXPERIMENTAL SETUP

The experimental setup is illustrated in Figure 1(a), including two cascaded Mamyshev fiber regenerators. The first regenerator consists of ~ 2 meters of double-cladding PM-YDF (Coherent PLMA-YDF-10/125-VIII) with a core/cladding diameter of 10/125 μm , forward cladding-pumped by a 9 W laser diode at 976 nm. It serves as a lower-energy feedback loop for the subsequent power-scaling arm. The second regenerator comprises ~ 2.4 meters of double-cladding PM-YDF (Coherent PLMA-YDF-25/250-VIII) with a core/cladding diameter of 25/250 μm , backward cladding-pumped by a 60 W laser diode at 976 nm through free space coupling optics. The fiber's V-number at 1.03 μm is calculated to ~ 5.1 , theoretically supporting four LP mode groups (LP₀₁, LP₁₁, LP₂₁, and LP₀₂). To ensure fundamental LP₀₁ mode exclusive operation, the

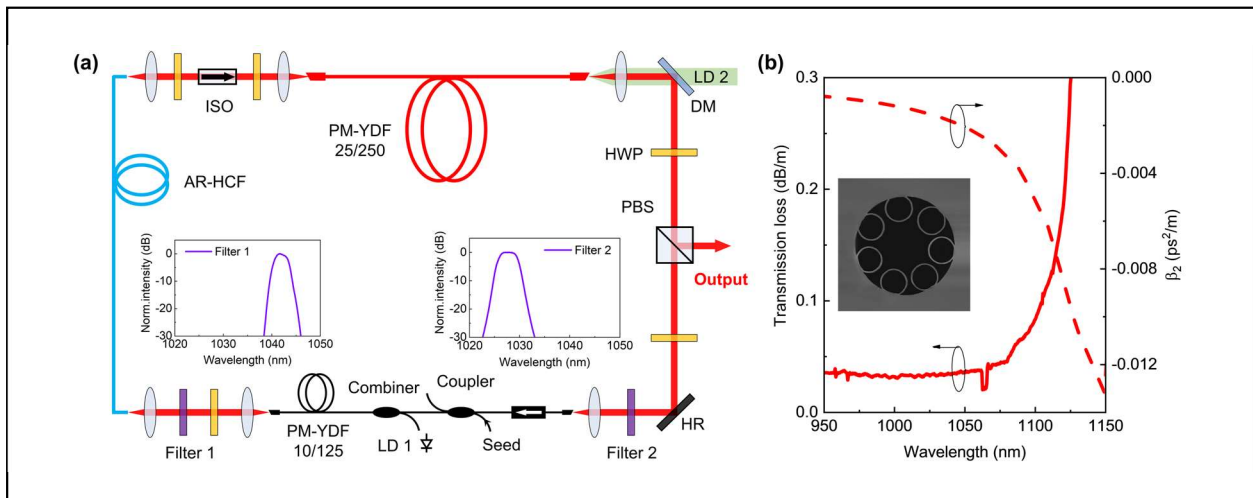


Figure 1. (a) Schematic of the experimental setup. DM, dichroic mirror; HR, high-reflection mirror; LD, laser diode. Inset: measured spectral transmission profiles of spectral filters. (b) Measured transmission loss (left axis) and calculated second-order dispersion β_2 (right axis) of the AR-HCF. Inset: SEM image of the fiber cross-section.

fiber is coiled with a bending diameter of 7 cm to introduce substantial losses to the higher-order modes. Numerical calculations reveal that the effective mode area of the LP₀₁ mode decreases from $\sim 360 \mu\text{m}^2$ in the straight fiber to $254 \mu\text{m}^2$ in the coiled configuration. Unlike conventional microjoule-scale MO architectures, this system employs two compact thin-film interference filters with near super-Gaussian transmission profiles for offset bandpass filtering, centered at 1042 nm with a full width at half maximum (FWHM) of 3 nm, and 1028 nm with a FWHM of 4.5 nm, respectively. The large spectral separation between the two filters results in a high modulation depth in the effective saturable absorber, thereby enabling the stable generation of high-energy pulses. Additionally, a slight narrower bandwidth of the spectral filter prior to the LMA-YDF facilitates the evolution of the pulse into a parabolic shape, leading to an improvement in the quality of the compressed pulse. A free-space PM isolator (PM-ISO) and a fiberized PM-ISO ensure unidirectional laser operation. A 2×2 PM-coupler with a power ratio of 90:10 is spliced to the signal input port of the pump/signal combiner, allowing the injection of external seed pulses via the 10% port to initiate the mode locking. In the second arm, a half-wave plate (HWP) combined with a polarization beam splitter (PBS) enables adjustable output coupling, which is set to 91% to maximize the energy of the output pulses. All solid-core fiber ends are spliced to appropriate silica endcaps with angle-polished end-facets for the ease of suppressing potential parasitic lasing.

Pre-chirp management is applied at the power-scaling arm by introducing variable lengths of AR-HCF or solid-core PM fiber (Coherent PM1060L) prior to the PM-YDF, providing either negative or positive GDD to the input pulses. Given the relatively low pulse energy after the spectral filter (~ 1.2 nJ), pulse propagation through the passive fiber is dominated by linear effects. The inset of Figure 1(b) shows a scanning electron microscope (SEM) cross-section image of the

self-fabricated AR-HCF, featuring a core diameter of 40 μm and a cladding formed by seven capillaries (20.8 μm inner diameter and 0.62 μm membrane thickness). Figure 1(b) depicts the measured transmission loss and calculated dispersion profiles of the AR-HCF. The transmission loss remains nearly constant at ~ 0.035 dB/m from 950 nm to 1080 nm, with a slight increase to 0.1 dB/m at 1115 nm. The calculated second-order dispersion β_2 is negative over the wavelength range, gradually decreasing with wavelength below 1080 nm (~ -0.004 ps²/m), and dropping more sharply to -0.012 ps²/m at 1150 nm.

III. RESULTS AND DISCUSSIONS

Mamyshev Oscillator characterization

A dispersion-managed mode-locked fiber laser serves as the seed source, providing an external signal to initiate the mode-locking. The seed laser exhibits a pulse duration of ~ 3 ps with a spectral bandwidth of 28 nm at the -10 dB level, sufficient to cover the passbands of two intracavity spectral filters. Seed pulses with an energy of ~ 55 pJ and a repetition rate of 26.08 MHz are injected into the first arm through the 10% port of the 10-dB PM-coupler. Reliable mode-locking of the MO is achieved, when the absorbed pump power at the power-scaling arm is increased to ~ 11.7 W, producing single output pulses with an energy of ~ 307 nJ at a repetition rate of 18.46 MHz. Once mode-locking is established, blocking the seed pulses can further enhance the stability of the mode-locked operation.

We gradually increase the pump power of the power-scaling arm to increase the output power of the MO. Figure 2(a) depicts the average output power and the corresponding pulse energy of the output pulses as a function of absorbed pump power, revealing a slope efficiency of $\sim 57\%$ with respect to the absorbed pump power. The MO can directly generate ~ 2.3 ps chirped pulses with a maximum average power of 9.84 W, corresponding to a single-pulse energy of ~ 533 nJ.

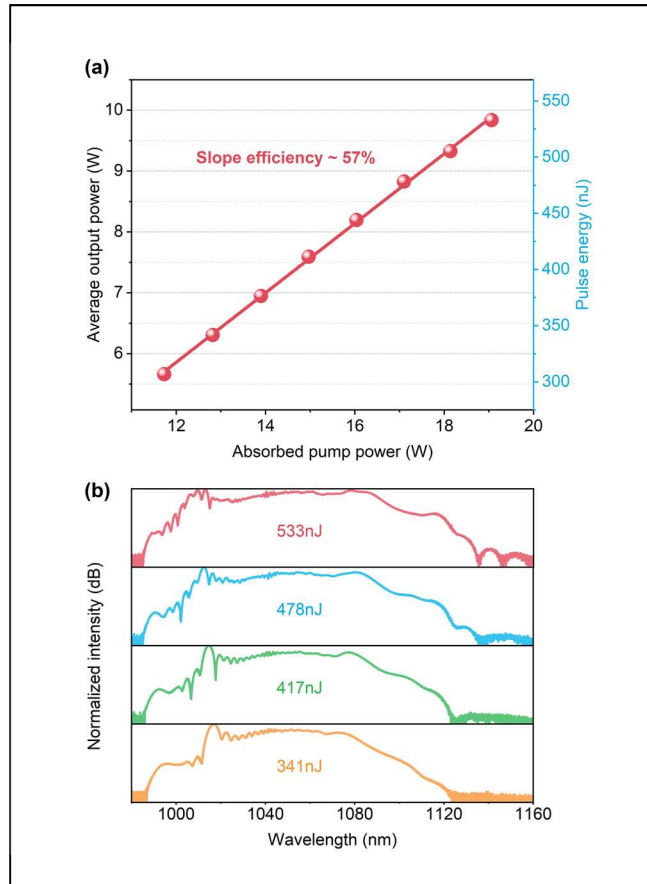


Figure 2. (a) Average output power (left axis) and pulse energy (right axis) as a function of absorbed pump power. (b) Measured output spectra for the indicated pulse energies.

This performance is comparable to that of MO employing the equivalent core-sized PM-YDFs with Gaussian-shaped spectral filters [31]. It is worth mentioning that the maximum achievable single-pulse energy in MOs is generally proportional to the effective mode field area (MFA) of the gain fibers within the cavity. Given that the MFA of the YDF in our study is only half that reported in references [6] and [7], the corresponding maximum single-pulse energy is also reduced by approximately half. Please note that the power of the first arm remains constant throughout the mode-locking process, leading to ~ 20 mW (~ 1.08 nJ) of spectrally filtered signal being injected into the second arm. Taking the signal coupling loss of ~ 1 dB into account, the second arm provides an effective gain of ~ 27.9 dB to achieve the maximum pulse energy. Figure 2(b) shows the measured output spectra of the second arm at variable pulse energies. As the output pulse energy

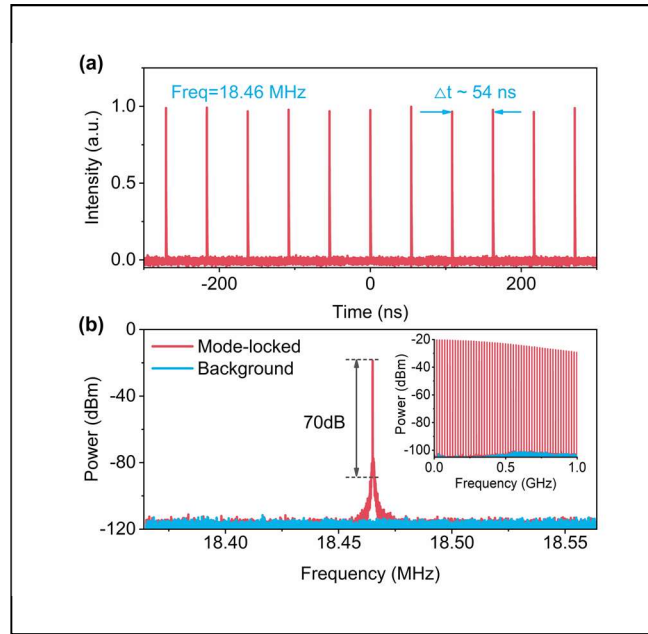


Figure 3. (a) Oscilloscope trace of the output pulses. (b) RF spectrum with a RBW of 10 Hz and a span of 200 kHz at the fundamental frequency of 18.46 MHz. Inset: RF spectrum with 1 GHz span.

increased, the spectral bandwidth at the -10 dB level gradually broadens from 66 nm to 89 nm (from 1005 nm to 1093 nm) due to the self-phase modulation (SPM) induced spectral broadening. The spectral profiles display asymmetry, primarily resulting from the self-steepening effect and pulse distortion induced by the third-order dispersion.

Figure 3(a) shows a typical pulse train with a repetition rate of 18.46 MHz, recorded by an oscilloscope (Lecroy WaveMaster 816Zi-B). The temporal stability of the output pulse train is further analyzed with a radio frequency (RF) spectrum analyzer (R&S FSW50). Figure 3(b) depicts the corresponding RF spectrum measured over a frequency span of 200 kHz, with a resolution bandwidth (RBW) of 10 Hz, showing a FWHM linewidth of ~ 40 Hz and a signal-to-noise ratio of ~ 70 dB, manifesting highly stable mode-locking with low pulse jitter. The inset of Figure 3(b) shows the RF spectrum measured over a 1 GHz span with a 100 Hz RBW, revealing no evidence of multiple pulsing.

Pre-chirp management

Each arm of the MO operates as a self-similar pulse amplifier, wherein the input pulse parameters play a crucial role in determining the characteristics of the output pulses. By precisely tailoring input parameters, such as pulse duration, spectral profile and pulse energy, the output pulses can be optimized to achieve maximal peak power after compression. Various experimental studies have demonstrated that pre-chirping the seed pulse can accelerate the convergence toward the parabolic regime in YDF amplifiers, thereby producing high-quality compressed output pulses. Accordingly, it is expected that applying pre-chirp to the power-scaling arm of the MO will be advantageous for generating linearly chirped output pulses at high pulse energies. In contrast to the conventional approach of employing a bulky diffraction grating pair to introduce pre-chirp in free space, which is impractical for all-fiber configurations, this work utilizes optical fibers of variable lengths to introduce controlled amounts of GDD. A 1-meter length of PM1060L fiber

with a core diameter 10 μm is positioned before the power-scaling arm to provide a GDD of ~ 0.022 ps^2 . In contrast, 2-meter and 4-meter lengths of AR-HCF are used to provide GDD values of ~ 0.004 ps^2 and ~ 0.008 ps^2 , respectively. It is noteworthy that nonlinear effects within these passive fiber sections are negligible due to the relatively low pulse energy of ~ 1.2 nJ, particularly in the case of AR-HCF. Figure 4(a) shows the measured output spectra at the maximum pulse energy of ~ 533 nJ for three experimental scenarios. The broader spectrum is observed at lower GDD values, which can be attributed to the accumulation of greater nonlinear phase shifts in the shorter-duration input pulses, leading to enhanced spectral broadening caused by SPM.

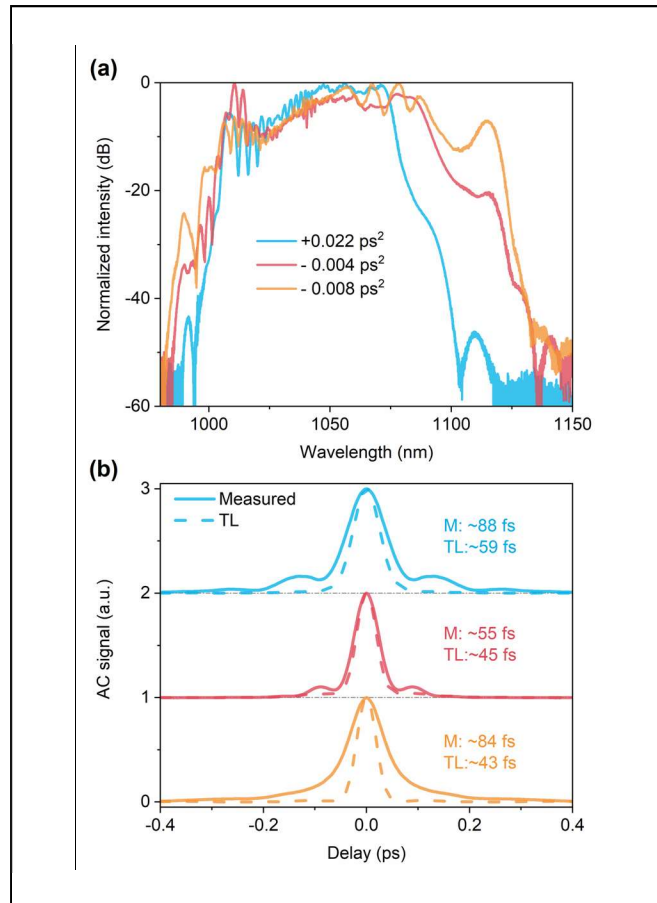


Figure 4. (a) Measured output spectra of the MO for GDD values of $+0.022$ ps^2 (blue), -0.004 ps^2 (red), and -0.008 ps^2 (orange) at the maximum pulse energy. (b) Corresponding measured AC traces of the dechirped pulses (solid curve) compared to the calculated AC traces of the TL pulses (dashed curve).

The output pulses are externally compressed by a pair of transmission gratings (1000 lines/mm) with a compression efficiency of $\sim 83\%$, resulting in a maximum dechirped pulse energy of ~ 442 nJ. Figure 4(b) depicts the measured intensity auto-correlation (AC) traces of the compressed output pulses for these three scenarios. The minimum AC duration is measured to ~ 55 fs when a GDD of ~ -0.004 ps² is applied. This corresponds to an AC duration that is ~ 1.23 times that of the TL pulse, indicating the generation of linearly chirped pulses. To the best of our knowledge, this represents the lowest ratio achieved in MOs employing super-Gaussian spectral filters, and it even surpasses the performance observed in most cases based on Gaussian spectral filters. Despite the presence of a minor pedestal, the AC trace can be accurately fitted with a series of individual Gaussian pulses, allowing for an estimation that $\sim 84\%$ of the total pulse energy is contained within the main pulse. Assuming a Gaussian-shaped pulse, the duration of the dechirped pulse is ~ 39 fs, corresponding to a peak power of ~ 9.7 MW. As shown in Figure 4(b), even a slight variation of GDD results in a substantial increase in the AC duration, revealing that the quality of pulse compression is highly sensitive to the GDD applied to the pulses seeding the power-scaling arm of the MO. Figure 5 illustrates the measured AC duration of dechirped pulses at different

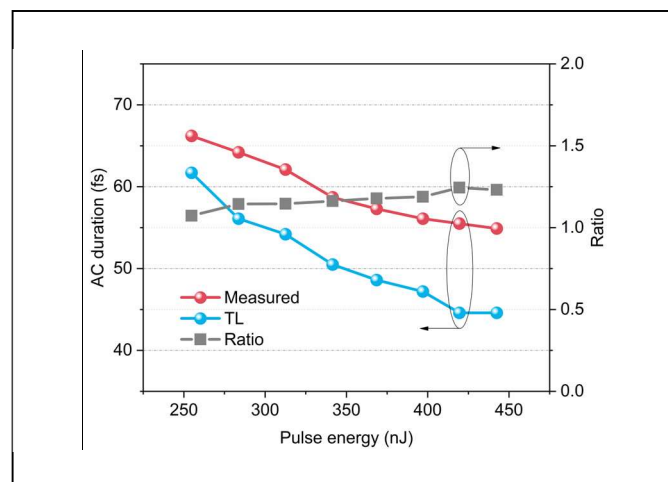


Figure 5. Measured AC duration of the dechirped pulses (red), calculated AC duration of the TL pulses (blue), and the corresponding ratio between the two (gray) as a function of increasing pulse energy.

compressed pulse energies. The AC duration decreases with the growing pulse energy due to the broadened output spectrum. Additionally, the ratio of AC duration to that of TL pulse exhibits a slight increase from 1.07 to 1.23 with a growing pulse energy, which can be attributed to the greater accumulation of uncompensated nonlinear phase shifts.

Pulse compression using an AR-HCF

We further investigate the potential of AR-HCF for ultrashort pulse compression, with a schematic of the experimental setup shown in Figure 6. The commonly used grating pair is replaced with an AR-HCF of the same type used within the cavity, providing anomalous dispersion to compensate for the positive chirp of the MO output pulses. Based on the pulse compression results achieved by the use of grating pair described in the above section, the GDD required to compress the output pulses at the maximum pulse energy of ~ 533 nJ is around -0.0235 ps². Consequently, an AR-HCF with a length of ~ 11.75 meters is employed, providing nearly equivalent GDD to that of grating pair. The output beam of the MO is first collimated to a spot size of ~ 1.4 mm, and subsequently focused to ~ 31 μm using an aspheric lens with a focal length of 32 mm to match the calculated fundamental mode field diameter of ~ 29 μm of the AR-HCF. This configuration yields a coupling efficiency of 90% when a 0.5-meter length of AR-HCF is involved. The ~ 11.75 -meter length of AR-HCF is loosely coiled with a bending diameter of ~ 50 cm, yielding a maximum compressed

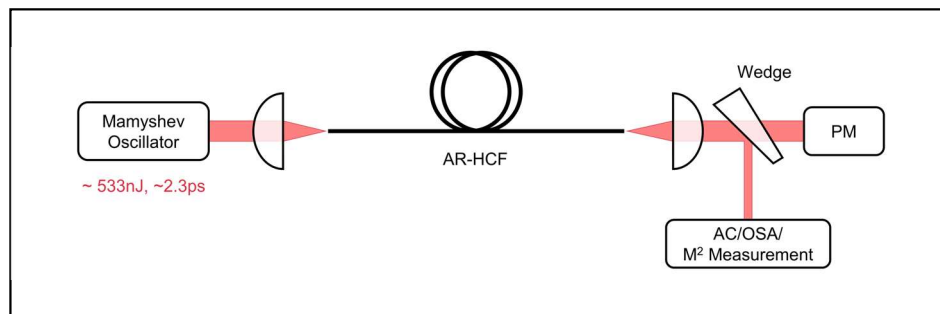


Figure 6. Schematic of the pulse compression setup utilizing the AR-HCF. PM, power meter; OSA, optical spectrum analyzer; AC, autocorrelator.

pulse energy of 432 nJ with an average output power of ~ 8.0 W at the fiber output, corresponding to an overall efficiency of $\sim 81\%$. It indicates that the transmission loss is approximately 0.04 dB/m taking into account the coupling loss. However, the overall throughput efficiency can be further improved through advancements in the design and fabrication of AR-HCFs. In addition, the polarization extinction ratio (PER) of the transmitted beam decreases from ~ 13 dB to ~ 9.7 dB, which can be attributed to the inherent non-polarization-maintaining characteristics of the AR-HCF.

The AC trace of the de-chirped pulse is measured with a FWHM duration of ~ 53 fs, while the corresponding TL pulse exhibited an AC duration of 43 fs, as shown in the red solid curve and blue dashed line in Figure 7(a), respectively. The AC duration is approximately equivalent to that achieved with the grating pair-based compressor, indicating effective compensation of second-order dispersion by the AR-HCF. While a slight pedestal is observed in the AC trace, it is estimated that the main lobe comprises $\sim 87\%$ of the total pulse energy. Assuming a Gaussian-shaped pulse, the duration of the dechirped pulse is estimated to ~ 37 fs, resulting in a peak power of approximately

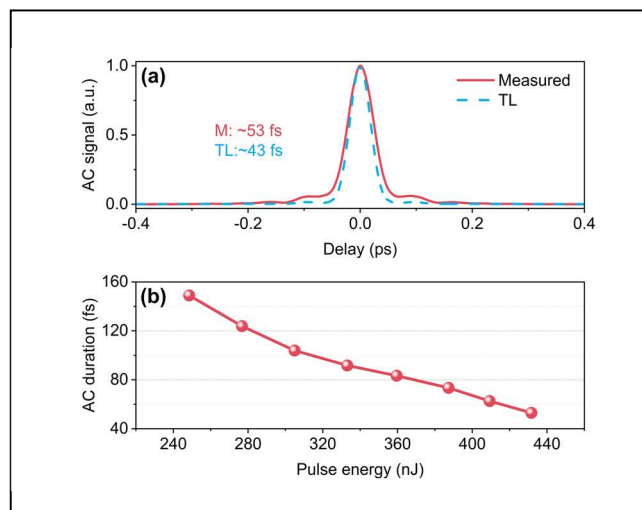


Figure 7. (a) Measured AC trace (solid red line) of the dechirped pulse and the calculated AC trace of the TL pulse (dashed blue line) using the AR-HCF. (b) Measured AC duration of the dechirped pulse as a function of pulse energies transmitted through the AR-HCF.

10 MW. If a more advanced AR-HCF with lower transmission loss is employed, this approach has the potential to achieve even higher peak power in this context. Figure 7(b) depicts the measured AC duration of the MO output pulses following propagation through the AR-HCF. It exhibits a monotonic decrease as pulse energy increases, consistent with our expectations. This phenomenon occurs because the required amount of GDD to compensate for the chirped pulses decreases as the pulse energy increases due to the gradual broadening of the spectral bandwidth.

The red curve in Figure 8(a) depicts the measured spectrum of the dechirped pulses, which shows only slight broadening compared to that of the MO output pulses with the blue curve. The close resemblance between both spectra suggests that the pulses experience only subtle nonlinear effects during the compression process. Figure 8(b) presents the beam quality (M^2) measurements at maximum pulse energy for the dechirped pulses from the AR-HCF, yielding $M_x^2 = 1.17$ and $M_y^2 = 1.13$. This result represents a slight improvement compared to the input beam ($M_x^2 = 1.18$ and $M_y^2 = 1.30$), indicating effective single-mode operation of the AR-HCF. The output beam exhibited a pronounced Gaussian-shaped intensity distribution in the far-field, as shown in the

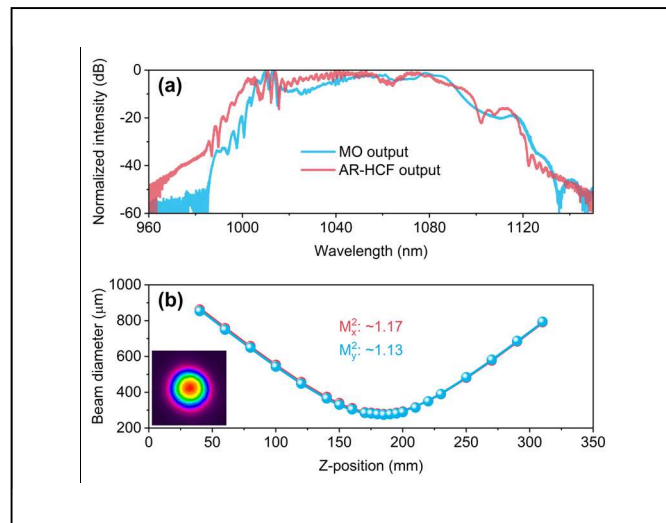


Figure 8. (a) Output spectrum of the MO (blue) and after AR-HCF delivery (red). (b) M^2 (beam quality) measurement at maximum pulse energy. Inset: measured far-field beam intensity profile.

inset of Figure 8(b). Notably, no fiber damage is observed throughout the extended duration of experimental characterization. Recent studies on picosecond pulse propagation through AR-HCFs have observed that spectral broadening due to self-phase modulation and stimulated Raman scattering becomes noticeable when the transmitted pulse accumulates a nonlinear phase shift of $\sim 3\pi$ [32,33]. In our experiment, the compressed pulse accumulates a nonlinear phase shift of $\sim 0.8\pi$, indicating that AR-HCFs can facilitate microjoule-level pulse compression within the linear regime, yielding peak powers in the range of several tens of megawatts. This technique is particularly advantageous for high-energy pulses generated by MOs and gain-managed fiber amplifiers, which typically exhibit broadband spectra and minimal linear chirp. Such pulses require reduced dispersion for dechirping, allowing for shorter fiber lengths and enabling higher peak powers for a given accumulated nonlinear phase shift.

IV. CONCLUSIONS

In conclusion, we have demonstrated a high-energy MO that incorporates several distinctive features, resulting in a streamlined system architecture while maintaining exceptional pulse performance. Conventional bulky grating-based spectral filters have been replaced with compact, fiber-integrable interferometric spectral filters. The deterioration in pulse compression quality, attributable to the detrimental effects of super-Gaussian spectral filters on pulse evolution, has been effectively mitigated through the pre-chirp management utilizing an appropriate length of AR-HCF. The air-filled AR-HCF, characterized by its anomalous dispersion and ultra-low nonlinearity, is further exploited as an extra-cavity linear pulse compressor to compensate for the linear positive chirp of the high-energy MO output pulses. This approach facilitated the flexible delivery of sub-40-fs pulses with peak power at the 10 MW level over a fiber length of ten meters. The results of this work represent a significant step toward the realization of a fully fiberized

monolithic MO capable of directly generating tens of megawatts of peak power at the fiber distal end over extended lengths. Such a laser source is expected to be highly desirable for a broad range of applications that demand the flexible delivery of high-peak-power femtosecond pulses to a designated target.

Acknowledgement

This work was supported by the National Key Research and Development Program of China (2022YFB2903102), National Natural Science Foundation of China (62335004, 62035002, U2241225), Guangdong Introducing Innovative and Entrepreneurial Teams of “The Pearl River Talent Recruitment Program” (2021ZT09X004).

References

1. M. E. Fermann, and I. Hartl, “Ultrafast fibre lasers”, *Nat. Photonics* 7, 868-874 (2013). DOI: <https://doi.org/10.1038/nphoton.2013.280>
2. K. Tamura, E. P. Ippen, H. A. Haus, and L. E. Nelson, “77-fs pulse generation from a stretched-pulse mode-locked all-fiber ring laser”, *Opt. Lett.* 18(13), 1080-1082 (1993). DOI: <https://doi.org/10.1364/OL.18.001080>
3. F. Ö. Ilday, J. R. Buckley, W. G. Clark, and F. W. Wise, “Self-similar evolution of parabolic pulses in a laser”, *Phys. Rev. Lett.* 92(21), 213902 (2004). DOI: <https://doi.org/10.1103/PhysRevLett.92.213902>
4. A. Chong, W. H. Renninger, and F. W. Wise, “All-normal-dispersion femtosecond fiber laser with pulse energy above 20 nJ”, *Opt. Lett.* 32(16), 2408-2410 (2007). DOI: <https://doi.org/10.1364/OL.32.002408>
5. Z. W. Liu, Z. M. Ziegler, L. G. Wright, and F. W. Wise, “Megawatt peak power from a Mamyshev oscillator”, *Optica* 4(6), 649-654 (2017). DOI: <https://doi.org/10.1364/OPTICA.4.000649>
6. W. Liu, R. Y. Liao, J. Zhao, J. H. Cui, Y. J. Song, C. Y. Wang, and M. L. Hu, “Femtosecond Mamyshev oscillator with 10-MW-level peak power”, *Optica* 6(2), 194-197 (2019). DOI: <https://doi.org/10.1364/OPTICA.6.000194>

7. D. Lin, D. Y. Xu, J. He, Y. T. Feng, Z. Q. Ren, R. Sidharthan, Y. M. Jung, S. Yoo, and D. J. Richardson, "The Generation of 1.2 μ J Pulses From a Mamyshev Oscillator Based on a High Concentration, Large-Mode-Area Yb-Doped Fiber", *J. Light. Technol.* 40(21), 7175-7179 (2022). DOI: <https://doi.org/10.1109/JLT.2022.3198737>
8. P. Sidorenko, W. Fu, L. G. Wright, M. Olivier, and F. W. Wise, "Self-seeded, multi-megawatt, Mamyshev oscillator", *Opt. Lett.* 43(11), 2672-2675 (2018). DOI: <https://doi.org/10.1364/OL.43.002672>
9. T. Wang, B. P. Ren, J. Wu, R. Su, P. Ma, Z. Luo, and P. Zhou, "Over 80 nJ Sub-100 fs All-Fiber Mamyshev Oscillator", *IEEE J. Sel. Top. Quantum Electron.* 27(6), 8800105 (2021). DOI: <https://doi.org/10.1109/JSTQE.2021.3094508>
10. H. W. Chen, J. K. Lim, S. W. Huang, D. N. Schimpf, F. X. Kärtner, and G. Q. Chang, "Optimization of femtosecond Yb-doped fiber amplifiers for high-quality pulse compression", *Opt. Express* 20(27), 28672-28682 (2012). DOI: <https://doi.org/10.1364/OE.20.028672>
11. J. Lim, H. W. Chen, G. Q. Chang, and F. X. Kärtner, "Frequency comb based on a narrowband Yb-fiber oscillator: pre-chirp management for self-referenced carrier envelope offset frequency stabilization", *Opt. Express* 21(4), 4531-4538 (2013). DOI: <https://doi.org/10.1364/OE.21.004531>
12. W. Liu, D. N. Schimpf, T. Eidam, J. Limpert, A. Tunnermann, F. X. Kartner, and G. Q. Chang, "Pre-chirp managed nonlinear amplification in fibers delivering 100 W, 60 fs pulses", *Opt. Lett.* 40(2), 151-154 (2015). DOI: <https://doi.org/10.1364/OL.40.000151>
13. J. Zhao, W. X. Li, C. Wang, Y. Liu, and H. P. Zeng, "Pre-chirping management of a self-similar Yb-fiber amplifier towards 80 W average power with sub-40 fs pulse generation", *Opt. Express* 22(26), 32214-32219 (2014). DOI: <https://doi.org/10.1364/OE.22.032214>
14. J. Yan, D. Xu, D. Lin, H. C. H. Mulvad, S. M. A. Mousavi, Y. Jung, D. Richardson, F. Poletti, and L. Xu, "Chirp-Managed, High-Energy, Low-Repetition Mamyshev Oscillator Based on Hollow Core Fiber", *Laser Photonics Rev.* 2401910 (2025). DOI: <https://doi.org/10.1002/lpor.202401910>
15. B. Debord, M. Alharbi, L. Vincetti, A. Husakou, C. Fourcade-Dutin, C. Hoenninger, E. Mottay, F. Gérôme, and F. Benabid, "Multi-meter fiber-delivery and pulse self-

- compression of milli-Joule femtosecond laser and fiber-aided laser-micromachining”, *Opt. Express* 22(9), 10735-10746 (2014). DOI: <https://doi.org/10.1364/OE.22.010735>
16. M. Andreana, T. Le, W. Drexler, and A. Unterhuber, “Ultrashort pulse Kagome hollow-core photonic crystal fiber delivery for nonlinear optical imaging”, *Opt. Lett.* 44(17), 1588-1591 (2019). DOI: <https://doi.org/10.1364/OL.44.001588>
17. A. Kudlinski, A. Cassez, O. Vanvincq, D. Septier, A. Pastre, R. Habert, K. Baudelle, M. Douay, V. Mytskaniuk, V. Tsvirkun, H. Rigneault, and G. Bouwmans, “Double clad tubular anti-resonant hollow core fiber for nonlinear microendoscopy”, *Opt. Express* 28(10), 15062-15070 (2020). DOI: <https://doi.org/10.1364/OE.389084>
18. A. Fernández, L. Grüner-Nielsen, M. Andreana, M. Stadler, S. Kirchberger, C. Sturtzel, M. Distel, L. Zhu, W. Kautek, R. Leitgeb, A. Baltuska, K. Jespersen, and A. Verhoef, “Optimizing pulse compressibility in completely all-fibered Ytterbium chirped pulse amplifiers for in vivo two photon laser scanning microscopy”, *Biomed. Opt. Express* 8(8), 3526-3537 (2017). DOI: <https://doi.org/10.1364/BOE.8.003526>
19. L. Andrus, H. Jeon, M. Pawlowski, B. Debord, F. Gerome, F. Benabid, T. Mau, T. Tkaczyk, and A. Ben-Yakar, “Ultrafast laser surgery probe for sub-surface ablation to enable biomaterial injection in vocal folds”, *Sci. Rep-Uk* 12, 20554 (2022). DOI: <https://doi.org/10.1038/s41598-022-24446-5>
20. K. Subramanian, I. Gabay, O. Ferhanoglu, A. Shadfan, M. Pawlowski, Y. Wang, T. Tkaczyk, and A. Ben-Yakar, “Kagome fiber based ultrafast laser microsurgery probe delivering micro-Joule pulse energies”, *Biomed. Opt. Express* 7(11), 4639-4653 (2016). DOI: <https://doi.org/10.1364/BOE.7.004639>
21. J. W. Nicholson, S. Ramachandran, S. Ghalmi, M. R. Yan, P. Wisk, E. Monberg, and E. V. Dimarcello, “Propagation of femtosecond pulses in large-mode-area, higher-order-mode fiber”, *Opt. Lett.* 31(21), 3191-3193 (2006). DOI: <https://doi.org/10.1364/OL.31.003191>
22. H. Lim, F. Ö. Ilday, and F. W. Wise, “Femtosecond ytterbium fiber laser with photonic crystal fiber for dispersion control”, *Opt. Express* 10(25), 1497-1502 (2002). DOI: <https://doi.org/10.1364/OE.10.001497>
23. T. Balciunas, G. Fan, S. Haessler, C. Fourcade-Dutin, T. Witting, A. A. Voronin, A. M. Zheltikov, F. Gérôme, G. G. Paulus, A. Baltuska, and F. Benabid, “Strong Field

- Applications of Gigawatt Self-compressed Pulses from a Kagome Fiber”, in *19th International Conference on Ultrafast Phenomena*, OSA Technical Digest (online) (Optica Publishing Group, 2014), paper 08.Tue.D.07.
24. J. Limpert, “High power pulse generation and compression with photonic crystal fibers”, in *Conference on Lasers and Electro-Optics*, OSA Technical Digest (Optica Publishing Group, 2016), paper SW4I.3.
25. M. Nisoli, “Hollow Fiber Compression Technique: A Historical Perspective”, *IEEE J. Sel. Top. Quantum Electron.* 30(6), 8900114 (2024). DOI: <https://doi.org/10.1109/JSTQE.2024.3373174>
26. X. M. Liu, J. Lægsgaard, and D. Turchinovich, “Highly-stable monolithic femtosecond Yb-fiber laser system based on photonic crystal fibers”, *Opt. Express* 18(15), 15475-15483 (2010). DOI: <https://doi.org/10.1364/OE.18.015475>
27. A. J. Verhoef, K. Jespersen, T. V. Andersen, L. Grüner-Nielsen, T. Flöry, L. Zhu, A. Baltuska, and A. Fernández, “High peak-power monolithic femtosecond ytterbium fiber chirped pulse amplifier with a spliced-on hollow core fiber compressor”, *Opt. Express* 22(14), 16759-16766 (2014). DOI: <https://doi.org/10.1364/OE.22.016759>
28. H. Sakr, Y. Chen, G. T. Jasion, T. D. Bradley, J. R. Hayes, H. C. H. Mulvad, I. A. Davidson, E. N. Fokoua, and F. Poletti, “Hollow core optical fibres with comparable attenuation to silica fibres between 600 and 1100nm”, *Nat. Commun.* 11, 6060 (2020). DOI: <https://doi.org/10.1038/s41467-020-19910-7>
29. H. C. H. Mulvad, S. A. Mousavi, V. Zuba, L. Xu, H. Sakr, T. D. Bradley, J. R. Hayes, G. T. Jasion, E. N. Fokoua, A. Taranta, S. U. Alam, D. J. Richardson, and F. Poletti, “Kilowatt-average-power single-mode laser light transmission over kilometre-scale hollow-core fibre”, *Nat. Photonics* 16, 448-453 (2022). DOI: <https://doi.org/10.1038/s41566-022-01000-3>
30. M. A. Cooper, J. Wahlen, S. Yerolatsitis, et al., “2.2 kW single-mode narrow-linewidth laser delivery through a hollow-core fiber”, *Optica* 10(10), 1253-1259 (2023). DOI: <https://doi.org/10.1364/OPTICA.495806>
31. D. Lin, D. Xu, J. He, Y. Feng, Z. Ren, and D. J. Richardson, “Generation of ~625 nJ pulses from a Mamyshev oscillator with a few-mode LMA Yb-doped fiber”, in

Conference on Lasers and Electro-Optics Europe and European Quantum Electronics Conference, OSA Technical Digest (Optica Publishing Group, 2021), paper cj_4_4.

32. S. A. Mousavi, H. C. H. Mulvad, N. V. Wheeler, P. Horak, J. Hayes, Y. Chen, T. D. Bradley, S. Alam, S. R. Sandoghchi, E. N. Fokoua, D. J. Richardson, and F. Poletti, “Nonlinear dynamic of picosecond pulse propagation in atmospheric air-filled hollow core fibers” ,*Opt. Express* 26(7), 8866-8882 (2018). DOI: <https://doi.org/10.1364/OE.26.008866>
33. W. Lu, X. Zhang, K. Zhu, K. Du, and P. Wang, “Propagation of High-Power Picosecond Pulse at 1064 nm Using Nodeless Anti-Resonant Hollow-Core Fibre”, *Chin. J. Lasers* 49(3), 0306001 (2022). DOI: <https://doi.org/10.3788/CJL202249.0306001>